

Rb1 Haploinsufficiency Promotes Telomere Attrition and Radiation-Induced Genomic Instability

Iria Gonzalez-Vasconcellos¹, Natasa Anastasov¹, Bahar Sanli-Bonazzi¹, Olena Klymenko¹, Michael J. Atkinson^{1,2}, and Michael Rosemann¹

Abstract

Germline mutations of the retinoblastoma gene (RBI) predispose to both sporadic and radiation-induced osteosarcoma, tumors characterized by high levels of genomic instability, and activation of alternative lengthening of telomeres. Mice with haploinsufficiency of the RbI gene in the osteoblastic lineage reiterate the radiation susceptibility to osteosarcoma seen in patients with germline RBI mutations. We show that the susceptibility is accompanied by an increase in genomic instability, resulting from RbI-dependent telomere erosion. Radiation exposure did not accelerate the rate of telomere loss but amplified the genomic instability resulting from the dysfunctional telomeres. These findings suggest that telomere maintenance is a noncanonical caretaker function of the retinoblastoma protein, such that its deficiency in cancer may potentiate DNA damage-induced carcinogenesis by promoting formation of chromosomal aberrations, rather than simply by affecting cell-cycle control. *Cancer Res;* 73(14); 4247–55. ©2013 AACR.

Introduction

The Fukushima nuclear accident has reawakened concerns about the long-term health consequences of radiation exposure, especially the risk of cancer and the contribution of individual genetic susceptibility to that risk. However, little is known about the cellular events that follow radiation exposure and lead to the development of cancer in a susceptible individual (1).

Osteosarcoma is a tumor that is readily induced by exposure to ionizing radiation, in particular through the deposition of α -particle emitting radionuclides in the mineralizing skeleton. This is reflected by the high osteosarcoma incidences in luminescent dial painters who ingested large quantities of radium salts (2), and in children treated with preparations of thorium (3). Exposure of the skeleton to external photon irradiation is also osteosarcomageneic, with this tumor being a frequent secondary cancer arising in radiation therapy fields (4).

Germline mutation of the *RB1* tumor suppressor gene increases sensitivity to both sporadic and radiation-induced osteosarcoma (5–7). A study of the genetic determinants that

Authors' Affiliations: ¹Institute of Radiation Biology, Helmholtz Zentrum München, Neuherberg; and ²Technische Universität München, Munich, Germany

Note: Supplementary data for this article are available at Cancer Research Online (http://cancerres.aacrjournals.org/).

Corresponding Author: Michael J. Atkinson, Institute of Radiation Biology, Helmholtz Center Munich, German Research Center for Environmental Health Institute of Radiation Biology, Ingolstaedter Landstrasse 1, 85764 Neuherberg, Germany. Phone: 49-89-3187-2983; Fax: 49-89-3187-3378; E-mail: atkinson@helmholtz-muenchen.de

doi: 10.1158/0008-5472.CAN-12-3117

©2013 American Association for Cancer Research.

predispose inbred mouse strains to radiation-induced osteosarcoma after injection of bone-seeking 227 Th revealed a major modifying gene mapping to the RbI locus (8). Analysis of the increased susceptibility to radiation that is associated with RbIis hindered by the high sporadic rate of cancer in animals engineered to lack one copy of RbI in the germline (9). However, the increased sensitivity to radiation could be reiterated in mice that had been rendered RbI haploinsufficient through the conditional deletion of one RbI allele in the osteoblastic lineage (6).

Osteosarcomas are characterized by the frequent activation of the alternative lengthening of telomeres pathway of telomere maintenance (10) and a high degree of genomic instability. As the loss of telomeric DNA may lead to karyotypic instability (11), and as RBI haploinsufficiency has been associated with increased genomic instability in premalignant retinoma cells (12), we postulate that the RbI gene may be the common denominator-linking susceptibility, genomic instability, and telomeric integrity. We report here that the loss of a single copy of the RbI gene is sufficient to cause sustained telomeric attrition and spontaneous genomic instability in cells of the osteoblastic lineage. The extent of the genomic instability is increased after exposure to radiation.

Materials and Methods

Animal breeding and conditional mutagenesis

FVB/N *Rb1*^{loxP/loxP} mice (13) were obtained from the NIH Mouse Models of Human cancer Consortium, whereas the FVB/N *COL1AI-Cre-Tg* mice (14) were obtained from the NIH Mutant Mouse Regional Resource Centre at UC Davis, California. The ROSA26R reporter mice B6: 129-*Gtrosa26*^{tm1Sor} (15) were purchased from the Jackson Laboratory, Maine. All animals were housed in facilities approved by the animal welfare committee of the State of Bavaria. The correct targeting

of the Cre expression to the osteoblastic lineage of *in vivo* was confirmed using (FVB/N *COLIAI-Cre-Tg* × B6:129-*Gtro-sa26* tm1Sor) mice (Supplementary Fig. S1). Inactivation of 1 allele of the *Rb1* gene in the osteoblastic lineage was achieved by mating FVB-*COLIAI-Cre-Tg* and FVB-*Rb1* lox $^{P/loxP}$ mice.

Primary osteoblast explant cultures

Long bones of 2- to 4-week-old offspring of FVB-COL1A1- $Cre-Tg \times FVB-Rb1^{loxP/loxP}$ mice were isolated as described previously (16). In brief, long bones were excised under sterile conditions and scraped free of adherent tissue. After removal of the epiphyses, the bone marrow was flushed using 1 mL PBS. Fragments of the cleaned bone were placed into 6-well dishes and cultured in 1 mL Dulbecco's Modified Eagle Medium supplemented with 10% fetal calf serum. After 1 week, the emergent osteoblastic cells were replated to give passage 1 (P1).

All cells were genotyped for Cre, Rb1, and the excised $RbI^{+/\Delta I9}$ locus (Supplemental Fig. S2A). For all studies, the wild-type $Rb^{+/+}$ and $RbI^{+/\Delta I9}$ cells used were Cre positive, unless specifically stated otherwise. As expected, no Cre mRNA transcripts were detectable in cultured osteoblasts (Supplemental Fig. S3) due to the repression of the collagen gene expression in the absence of differentiation-promoting medium supplements (16).

Senescence-associated B-galactosidase assay

The assay was conducted using the β -gal staining kit (Sigma-Aldrich) according to the manufacturer's instructions.

Micronuclei assay. The presence of DNA micronuclei fragments was quantified using a standard protocol (17). A total of 250,000 cells were seeded onto glass microscope slides and 24 hours later were irradiated with either 2 or 4 Gy using an Isovolt 200 X-ray device operating at 230 kVp and 20 mA, with a 1 mm Al and 0.5 mm Cu filter. Sham-irradiated cells were handled in the identical manner without exposure to the X-irradiation. Cytochalasin B (0.5 μ g/mL) was added to the cultures for 18 hours at time 0 after irradiation to block the next cytokinesis. Cells were subsequently fixed in 80% ethanol for 15 minutes. DNA was visualized using 4',6-diamidino-2-phenylindole (DAPI) staining (150 ng/mL) for 5 minutes. Slides were washed in distilled H₂O, air-dried and coverslip mounted using 1 drop of Vectashield. Scoring of micronuclei in binucleate cells was done according to the HUMN project protocols.

Quantification of anaphase bridges. The fidelity of chromosomal segregation was determined by visualization of the chromatin in postmitotic cells. A total of 250,000 cells per glass slide were irradiated 24 hours after seeding at 0, 2, and 4 Gy. Cells were grown for a further 48 hours to allow at least 4 cell divisions (cycle time of approximately 12 hours). After fixation in 80% methanol for 15 minutes, the slides were stained with Hoechst 33342 for 5 minutes, washed twice with PBS, and coverslip mounted with 1 drop of Vectashield. Scoring was done visually by counting the number of bridges per 250 cells. Each cell revealing a spontaneous or radiation induced anaphase bridge was scored once, even if multiple bridges existed within that cell. Chromatin bridges between 2 postmitotic daughter cells were also scored and were considered to belong to 1 parental cell.

Propidium iodide labeling for FACS analysis of the cell cycle. Cells were trypsinized, washed with 5 mL PBS, and spun down at 1,400 rpm for 5 minutes 5 mL of 70% ethanol (cold) was added while gently vortexing and left in ethanol at 4°C for 4 hours. The fixed cells were spun down at 1,400 rpm for 5 minutes and resuspended 475 μ L PBS, plus 3.3 μ L RNAse (30 mg/mL) and 25 μ L propidium iodide (1 mg/mL). Cell-cycle analysis was conducted using a FACSCoulter (Becton Dickinson).

Telomeric staining by in situ *FISH*. Telomere length was determined by in situ FISH labeling of genomic DNA (18). Chromosome spreads or interphase nuclei were prepared by incubating cells with 0.05 $\mu g/mL$ Colcemid for 6 hours. Cells were harvested, incubated in 0.056 M KCl at 37°C for 10 minutes and fixed in methanol/acetic acid (3:1). Metaphase chromosomes were spread on glass slides, air dried overnight, and fixed in 4% formaldehyde in 1 \times PBS for 4 minutes. To conduct the hybridization, the samples were treated with 100 $\mu g/mL$ RNase A in 2 \times single-strand conformational polymorphism at 37°C for 1 hour, dehydrated through an ethanol series (70%, 85%, and 100% ethanol for 4 minutes each) at room temperature and air dried. A hybridization mixture (70% formamide, 0.5% bovine serum albumin (BSA), 10 mmol/L Tris-HCl (pH 7.2) and 0.5 µg/mL fluorescein isothiocyanate (FITC) conjugated (C₃TA₂)₃ peptide nucleic acid (PNA) probe (PANAGENE) was applied onto the slides. DNA was denatured at 75°C for 5 minutes. Hybridizations were carried out at room temperature for 4 hours. Slides were washed 2×15 minutes in 70% formamide, 10 mmol/L Tris-HCl (pH 7.2) and 3 \times 5 minutes in 0.1 M Tris-HCl, 0.15 M NaCl, 0.08% Tween-20 (pH 7.5) at room temperature. Slides were covered with one drop of Vectashield (containing 100 ng/mL DAPI for counterstaining) and mounted with a coverslip.

Telomere length measurement by flow cytometry (Flow-*FISH*). FISH-labeled telomeres were quantified as previously described (19). Primary cells in culture were washed in PBS and centrifuged, the supernatant was discarded and 500.000 cells resuspended in 500 µL of hybridization mixture containing 70% deionized formamide, 20 mmol/L Tris buffer, pH 7, 1% BSA, and 0.3 µg/mL of the FITC-conjugated PNA probe. Samples were denatured for 10 minutes at 80°C and left to hybridize for 3 hours in the dark at room temperature. Samples without PNA probe were used as negative control. Excess probe was removed in a wash solution containing 70% formamide, 10 mmol/L Tris buffer (pH 7), 0.1% BSA, and 0.1% Tween-20 followed by 2 washes in PBS, 0.1% BSA, and 0.1% Tween-20. Cells were then incubated in 500 μ L PBS, 0.1% BSA, 10 μ g/mL RNAse A, and 0.1 µg/mL propidium iodide for 1 hour at 4°C before analysis. All samples were stored on ice until analysis by flow cytometry.

Analysis was done on fresh samples using a FACSCoulter (Becton Dickinson). The FITC signal was detected in the green channel and the propidium iodide fluorescence in the red channel with no compensation set on the instrument.

Lentiviral expression vectors. RB1-expressing lentivirus (LV-RB1) was produced by polymerase chain reaction (PCR) amplification of the RB1 cDNA insert of cDNA clone MGC 29887 (Life Technologies). The insert was cloned into the lentiviral vector (pCDH-EF1-MCS-T2A-copGFP; Biocat). The

Rb1 shRNA-expressing lentivirus (LV-shRb1) was generated by insertion a short hairpin sequence targeting *Rb1* (GCTTAAAT-CAGAAGAAA) into the pFUGW plasmid (20). Control shRNA lentivirus (LV-scr) was generated using a scrambled sequence (Dharmacon Research). Constructs were sequenced to confirm error-free amplification before transduction. Creexpressing lentivirus under the control of the cytomegalovirus (CMV) promoter with a green fluorescent protein (GFP) expression cassette (LV526) for transduction control was purchased from GenTarget. In this case, the control lentivirus expressed only the GFP mRNA (LV-GFP).

Production of lentivirus was done as recently described (21). For all lentiviral transductions, we used a multiplicity of infection of 2 (2 \times 10^5 cells per well and 4 \times 10^5 TU/mL). Transduction efficiency was determined 72 hours after infection by flow-cytometric analysis of GFP-positive cells. Three or 4 days after infection cells were analyzed by reverse-transcriptase (RT)-PCR and Western blotting to ensure efficacy of the expression.

Analysis of status of genes involved in osteosarcomagenesis in *ex vivo* cultured osteoblast cells

The coding sequences of *Rb1*, *Cdkn2a/Arf*, and *p53* were amplified from cDNA and subjected to cycle sequencing using the BigDye 3.1 kit (Applied Biosystems). *Mdm2* gene copy

number was determined by real-time quantitative PCR of genomic DNA (SybrGreen; Applied Biosystems). Relative copy numbers of Mdm2 were calculated by the $\Delta\Delta C_t$ method, using normal mouse tissue as the diploid reference. The primers used for amplification and sequencing are listed in the Supplementary Material.

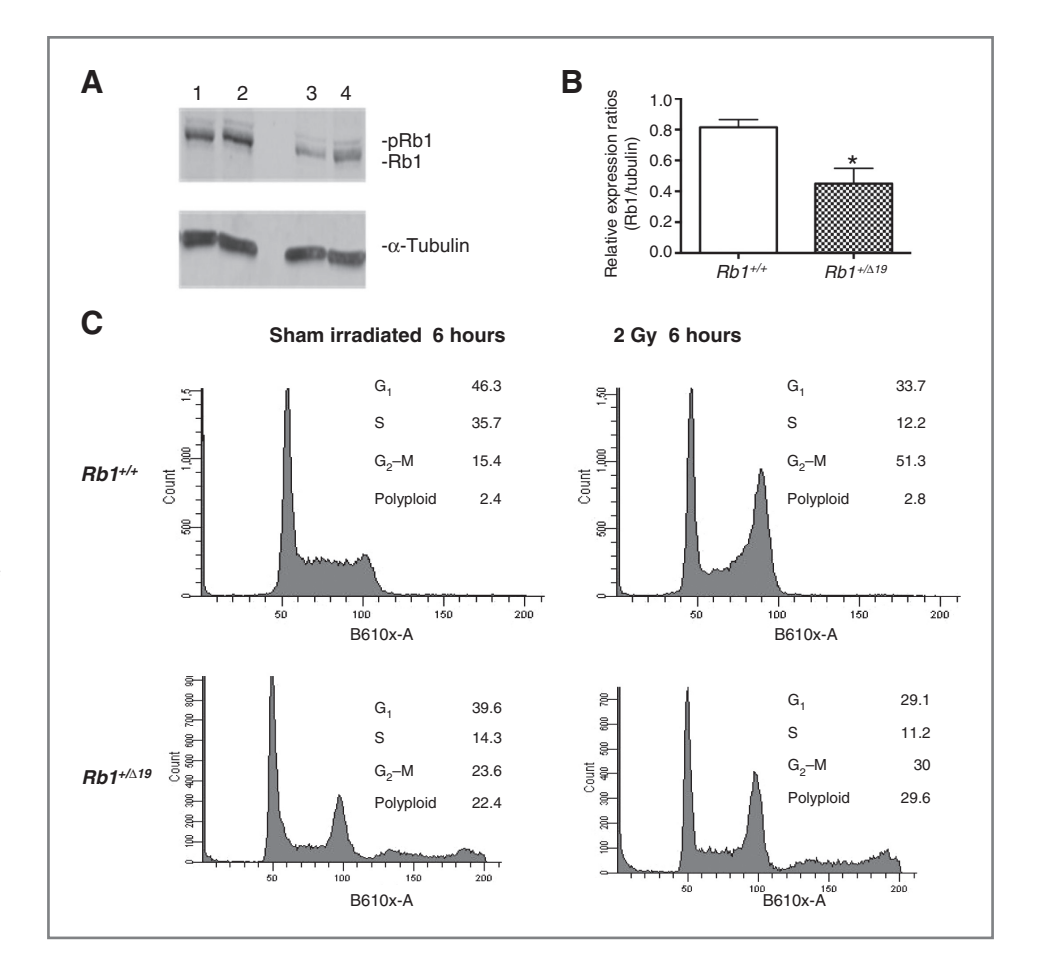
Results

Haploinsufficiency of *Rb1* leads to dysfunctional cellcycle arrest and senescence following radiation exposure

To confirm the conditional deletion of 1 Rb1 allele and the expected haploinsufficiency, we used exon-specific PCR to amplify both wild-type and exon 19-deleted copies of the *Rb1* gene. The content of the wild-type *Rb1* allele was almost halved in cells where the exon 19-deleted allele was present (Supplementary Fig. S2A). The same change was evident at both the transcriptional (Supplementary Fig. S2C) and translational levels (Fig. 1A and B) confirming haploinsufficiency. No reduction of the remaining wild-type *Rb1* allele was evident, even after 22 continual passages (Supplementary Fig. S2B).

As expected from the known tumor suppressor role of Rb1 in cell-cycle regulation, the reduced level of Rb1 altered the cell-cycle kinetics, with a reduced number of cells present in both the G_1 and S phases assayed by flow cytometry (Fig. 1C). The presence of a large fraction of polyploid cells may account for

Figure 1. A, detection of Rb1 protein expression. Top, Rb1 Western blot analysis conducted with anti-Rb1 (Becton and Dickinson). Lanes 1 and 2 are biological replicates of wild-type cells; lanes 4 and 5 are biological replicates of $Rb1^{+/\Delta 19}$ cells. Bottom, blot labeled with antitubulin as loading control. B, Rb1 protein quantification of Rb1 in primary osteoblasts from 3 biological replicates with 2 technical replicated each. A reduction of the Rb1 protein levels of 50% is observed in $Rb1^{+/\Delta18}$ cultures (t test, *, $P \le 0.01$). C, cell-cycle analysis of Rb1+/- $Rb1^{+/\Delta19}$ cells. A representative FACS-based cell-cycle analysis of sham- and 2 Gy-irradiated cells at passage 6 that were harvested 6 hours after radiation exposure. Cell-cycle distribution analysis was conducted by setting a fixed gate for each phase of the cell cycle. Impairment of the ability of irradiated $Rb1^{+/\Delta 19}$ osteoblasts to block cell-cycle progression in G₁-S and to arrest in G₂-M were detected.



this shift as the population doubling time remained unaffected. A functional deficit in the cell-cycle checkpoints was evident following a challenge with 2 Gy acute irradiation. In wild-type cells, the expected rapid G_2 –M arrest after irradiation was evident, but was severely abrogated in haploinsufficient $RbI^{+/\Delta I9}$ cells (Fig. 1C). This was associated with a further increase in the polyploid fraction but not the appearance of a sub- G_0 apoptotic fraction. Cell stress induced by the exposure to ionizing radiation effectively induced senescence of wild-type cells in a dose-dependent manner. However, the induction of senescence was diminished in haploinsufficient cells, even following a 4 Gy exposure (Fig. 2A).

Rb1 haploinsufficiency is associated with sporadic increases in micronuclei formation and the polyploid cell fraction

Possible alterations in the stability of the genome in Rb1 haploin sufficient cells were studied by examining micronuclei and polyploidy. The number of spontaneous micronuclei (acentric fragments of genomic DNA; Fig. 2B) was elevated in $RbI^{+/\Delta I9}$ cells when compared to RbI proficient wild-type cells. As with the polyploid fraction, the number of cells showing micronuclei rose with increasing passage number. Polyploid cells were also present in wild-type osteoblasts, where they also showed an increase in numbers at higher passages (Fig. 2C). In contrast, the size of the polyploid cell fraction in haploin sufficient wild-type osteoblasts, where they also showed an increase in numbers at higher passages (Fig. 2C). In cient $RbI^{+/\Delta I9}$ cells increased dramatically with increasing passage numbers, comprising almost 25% of the population by passage 12 (Fig. 2C). Even though we are unable to definitively determine the origin of the polyploid cells a dot plot of cell size versus DNA content of the haploin sufficient cells indicates that a small percentage of the measured G_2 –M population are possibly an uncertain overlap of tetraploid G_1 cells.

The spontaneous genomic instability of the *Rb1* haploinsufficient cells is accompanied by increased telomere attrition

The stability of telomeric regions is associated with loss of genome stability. We therefore quantified telomeric integrity after loss of 1 Rb1 allele. Labeling of telomeric DNA sequences with the fluorescent Cy3-PNA telomeric DNA probe revealed the presence of telomeric DNA within the micronuclei in both wild-type and $Rb1^{+/\Delta 19}$ cells at passage 11. The Rb1 haploin-sufficient cells exhibited more than 2 times the number of telomere-positive micronuclei than the wild-type cells (Fig. 2D). An examination of interphase cells indicated an overall reduction in the level of PNA-labeled telomeric sequences in $Rb1^{+/\Delta 19}$ cells, compared to their wild-type counterparts. Labeling of metaphase spreads revealed that the decrease in telomeric signal strength was due to a general reduction in signal intensity and to the development of considerable

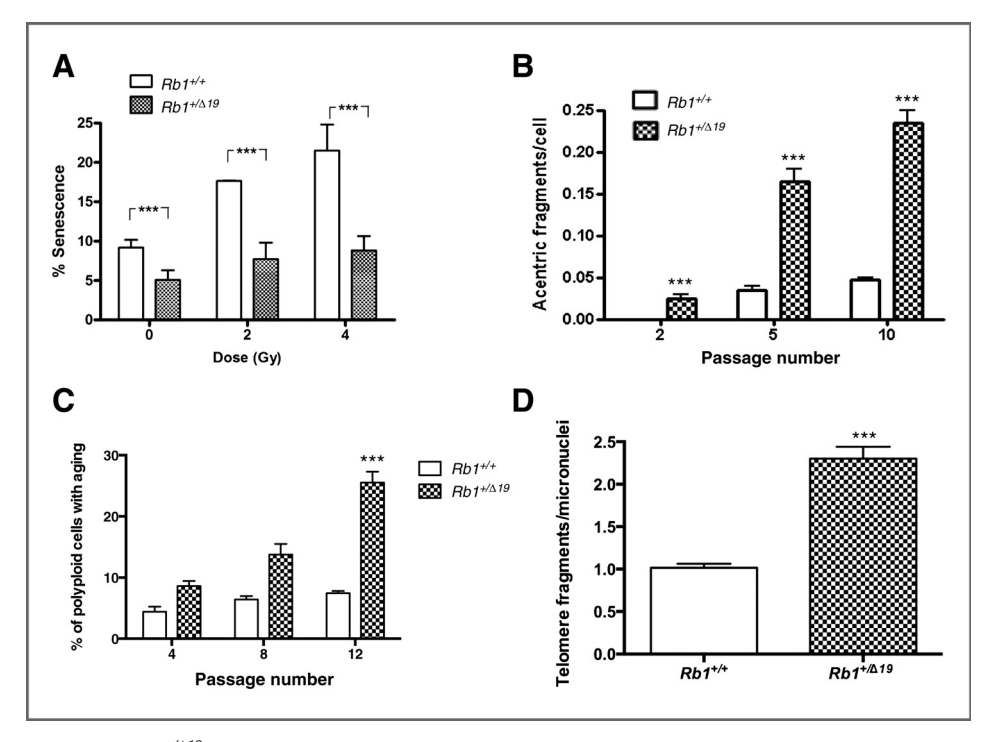


Figure 2. Genomic instability in $Rb1^{+/\Delta19}$ osteoblasts. A, entry of irradiated cells into senescence. Radiation exposure was associated with the appearance of the senescence marker SA-βGal in wild-type cells, but no increase in senescent cells was observed in irradiated $Rb1^{+/\Delta19}$ osteoblasts. Three biological replicates with 3 technical replicates each were used. B, quantification of acentric DNA fragments per cell after increasing passages. Data are from 2 biological replicates. Note that at passage 2 no fragments were detectable in wild-type cells. C, changes in the polyploid population of $Rb1^{+/L19}$ cells. Changes in the polyploid fraction at increasing passage numbers. Data are from 2 biological replicates. D, telomeric fragments present in micronuclei (acentric fragments). The presence of PNA-positive telomeres signals per 200 acentric DNA fragments in wild-type and $Rb1^{+/\Delta19}$ cells. Two biological replicates at passage 11. ***, P < 0.001 using Student's t test.

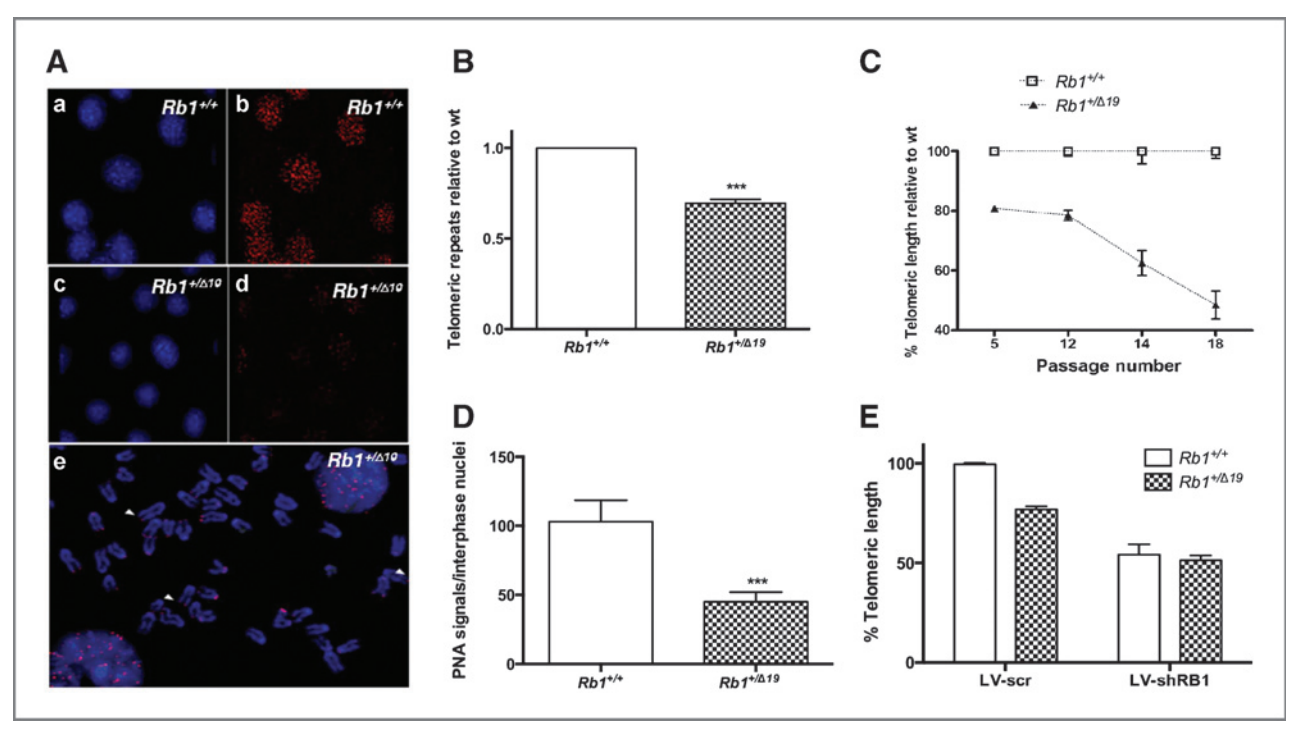


Figure 3. Increased telomere attrition in Rb1 haploinsufficient primary mouse osteoblasts. A, representative images (\times 40) from cell lines that were established from 2 animals. a and b, wild-type cells at passage 8; c–e, haploinsufficient cells ($Rb1^{+/\Delta19}$) at passage 8. DAPI nuclear staining is shown in a and c, whereas PNA-Cy3 telomeric labeling is depicted in b and d. Representative metaphase spreads of haploinsufficient cells ($Rb1^{+/\Delta19}$) at passage 8 are shown in e. Heterogeneous telomeric signal intensity was detected by PNA-Cy3 labeling counterstained with DAPI. Solid arrowheads indicate examples of chromatids with different signal intensities. B, quantitative genomic PCR measurement of average telomeric repeats. A global PCR amplification of telomeric sequences was conducted using (TTAGGG)n primers. The anonymous locus D14-192 (microsatellite flanking region) was used for normalization of genomic DNA content. $Rb1^{+/\Delta19}$ cells showed a decrease in telomere length of 30% at passage 10, which correlated with the results using Flow-FISH. Data represent mean \pm SD of 3 biological replicates. C, the telomeric length of $Rb1^{+/\Delta19}$ cells was measured by Flow-FISH counting of 20,000 cells. The length relative to wild-type cells of the same passage was followed over consecutive passages. Data are from 2 biological replicates. D, average of PNA signals in interphase nuclei for $Rb1^{+/\Delta19}$ counted in 100 interphase nuclei. Data from 2 biological replicates. E, Rb1 knockdown. Telomeric length assayed by Flow-FISH (20,000 cells) at the third passage of cells infected at passage 5 with either control lentivirus (LV-scr) or shRB1-expressing lentivirus (LV-shRB1). Data are from 2 biological replicates. ****, P < 0.001 using Student's t test.

heterogeneity in the labeling intensity of different chromosomes in $RbI^{+/\Delta I9}$ primary osteoblastic cells (Fig. 3A).

Assay of telomere length using quantitative genomic PCR amplification (Fig. 3B and C) established that there was a global reduction in telomere repeats in the $Rb1^{+/\Delta 19}$ cells that coincided with the reduced PNA labeling. As with the parameters describing genomic instability, the reduction in the average telomere lengths of $Rb1^{+/\Delta 19}$ cells grew larger with subsequent passages compared to wild-type cells. The mean number of 102 telomeres detected in wild-type cell at passage 8 approached the theoretical mean value of 108 telomeres that would be expected, taking into account the relative numbers of diploid and tetraploid cells we observed in asynchronous cultures. The number of distinct PNA-labeled telomeres in $Rb1^{+/\Delta 19}$ cells was reduced by more than half (Fig. 3D).

Telomeric loss is induced by shRNA-mediated knockdown of *Rb1* expression

To confirm that the engineered Rb1 haploin sufficiency is indeed responsible for the observed changes, we studied the effect of a direct knockdown of Rb1. Wild-type and haploin sufficient $Rb1^{+/\Delta 19}$ cells were transduced with the LV-shRb1lentivirus, This lead to the expected reduction in Rb1 expression (Supplementary Fig. S4) and was associated with a reduction in telomere length as early as the third passage post-transduction in both wild-type and haploin sufficient cells, compared to the same cells transduced instead with the LV-scr control lentivirus (Fig. 3E). The decrease in telomere length was more pronounced when LV-shRb1 was used to further deplete the already reduced Rb1 expression of the Rb1 $^{+/\Delta19}$ cells (Fig. 3E).

Transduction of Cre negative wild-type $(Rb1^{+/+})$ cells and of Cre negative cells containing a nondeleted floxed Rb1 allele $(Rb1^{+/flox})$ with the Cre-expressing lentivirus resulted in *in vitro* Cre expression (Supplementary Fig. S5). Telomere shortening was observed in the Cre-expressing primary osteoblasts containing the nondeleted floxed Rb1 allele $(Rb1^{+/flox})$ but not in the Cre-expressing wild-type $(Rb1^{+/+})$ cells 3 passages after transduction (Supplementary Fig. S6).

Telomere loss and genomic instability in $RbI^{+/\Delta I9}$ haploin sufficient cells are prevented by expression of

As a final proof of the role of Rb1 in telomere maintenance, we followed telomeric status after restoration of Rb1 expression. The accelerated rate of telomere loss in $Rb1^{+/\Delta I9}$ cells

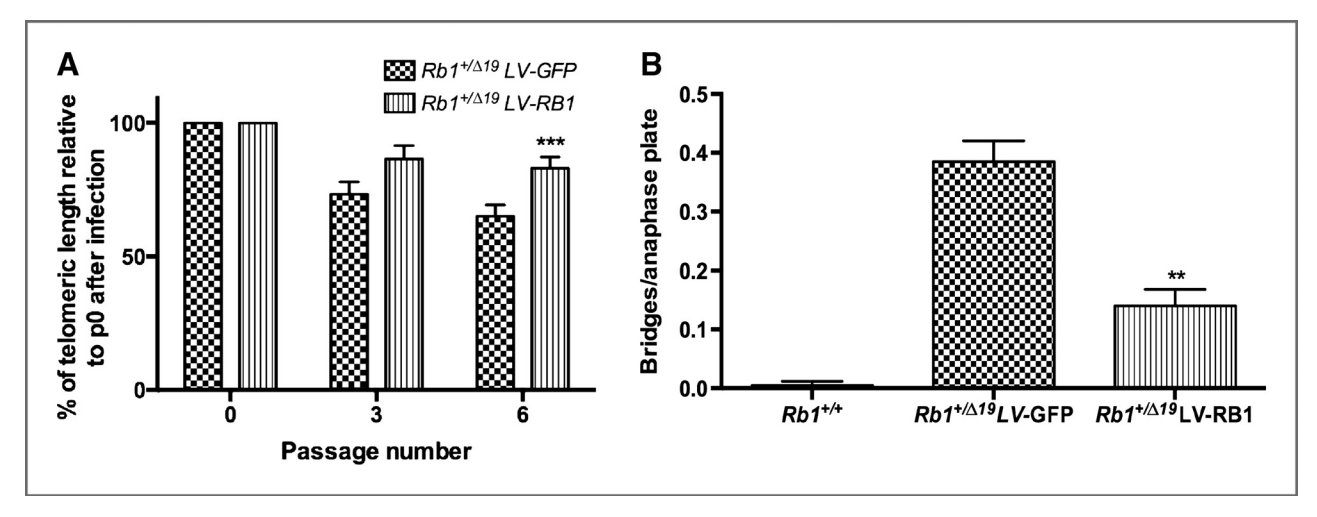


Figure 4. Rescue of the *Rb1* genotype leads to buffered telomeric loss. A, *RB1* expression. Telomere length was quantified by Flow-FISH at 0, 3, and 6 passages after transfection of passage 8 cells using the LV-RB1 lentivirus. Hatched columns are $Rb1^{+/\Delta19}$ cells infected with control lentivirus (LV-GFP) and vertical barred columns are $Rb1^{+/\Delta19}$ cells transfected with LV-RB1. Data are from 2 biological replicates. B, anaphase bridges quantification. Bridges per 100 anaphase plates measured 6 passages after infection with LV-RB1. Data are from 2 biological replicates at passage 6. ** and ****, P < 0.001 using Student's t test.

could be prevented by transduction with LV-RB1 lentivirus whereas transduction with control LV-GFP lentivirus had no effect, with telomere shortening continuing unabated (Fig. 4A). The expression of RB1 in the haploinsufficient $Rb1^{+/\Delta 19}$ cells rescued the increased level of sporadic genomic instability, as measured by the number of anaphase bridges per metaphase plate (Fig. 4B). The expression of RB1 following transduction was equivalent to that of endogenous Rb1 in wild-type cells (Supplementary Fig. S7) and did not cause cell-cycle arrest. Thus, the proportion of cells in G_1 , S_1 , and G_2 -M phase were comparable to those of wild-type cells at the same passage (38.5%, 21.5%, and 40% vs. 39.6%, 22.8%, and 37.6%).

Telomere attrition is not a consequence of changed oncogene/suppressor gene activity

The direct sequencing of the p53, Cdkn2a/Arf, and the remaining wild-type Rb1 allele in $Rb1^{+/\Delta 19}$ cells at the 12th passage did not reveal any alterations in the coding regions of these genes. In addition, the copy number of the Mdm2 oncogene was shown to be the same as that found in wild-type tissue (Supplementary Fig. S8). P53 expression was undetectable in wild-type and haploinsufficient $Rb1^{+/\Delta 19}$ cells, but in a subclone of apparently spontaneously transformed cells detected in long-term cultures of $Rb1^{+/\Delta 19}$ cells, we were able to detect a point mutation in exon 8 of the p53 gene, leading to accumulation of immunoreactive p53 protein (Supplementary Fig. S9).

Radiation exposure increases genomic instability of Rb1 haploinsufficient cells

The double-strand breaks induced by ionizing radiation may promote genomic instability in cells already rendered susceptible by lack of telomeres. Consequently, we exposed haploin-sufficient $Rb1^{+/\Delta 19}$ cells to an acute dose of radiation. The exposure to ionizing radiation caused cytogenetic abnormalities (micronuclei) in equal numbers of wild-type and haploin-

sufficient $Rb1^{+/\Delta I9}$ cells 24 hours after exposure, attesting to the uniformity of the radiation field (Supplementary Fig. S10; Fig. 5A). However, the number of micronuclei induced in 2 Gy irradiated haploinsufficient $Rb1^{+/\Delta I9}$ cells greatly exceeded that induced by the same exposure in wild-type cells (Fig. 5B) from 1.45 \pm 0.13 in the wild-type to 2.2 \pm 0.26 in the haploinsufficient cultures. The number of radiation-induced anaphase bridges in $Rb1^{+/\Delta I9}$ cells was more than 4-fold higher than that in irradiated wild-type cells (Fig. 5C). The size of the polyploid cell fraction was also increased by radiation exposure in both wild-type and $Rb1^{+/\Delta 19}$ cells. The number of polyploid cells arising in the irradiated haploin sufficient $Rb1^{+/\Delta I9}$ cells was considerably greater (29.6%) than that seen in the irradiated wild-type cells (2.8%; Fig. 5D). Importantly, the radiation exposure did not influence the telomere length in either the wild-type or haploinsufficient cells (Fig. 5E). Telomeric DNA was present in both acentric fragments (micronuclei) and anaphase bridges (Fig. 5F), indicating involvement of the truncated telomeres in the radiation-induced increase in genomic instability.

Discussion

Loss of one copy of the retinoblastoma gene (RB1) increases predisposition to the development of both sporadic and radiation-induced osteosarcoma (4, 22). The increase in sensitivity to radiation-induced osteosarcoma is reiterated in a mouse model upon conditional inactivation of the Rb1 gene in the osteoblastic lineage (6). We now show that loss of only one Rb1 allele in nontransformed primary osteoblast cell cultures is accompanied by a number of hallmarks of genomic instability. Thus, in $Rb1^{+/\Delta I9}$ cells, as well as in cells where the endogenous Rb1 expression was suppressed by shRNA, we observe the appearance of a polyploid cell fraction, the presence of sporadic micronuclei (acentric DNA fragments), and extreme shortening of the telomeric DNA. Restoration of the Rb1 status by lentiviral expression of the human RB1 gene was sufficient

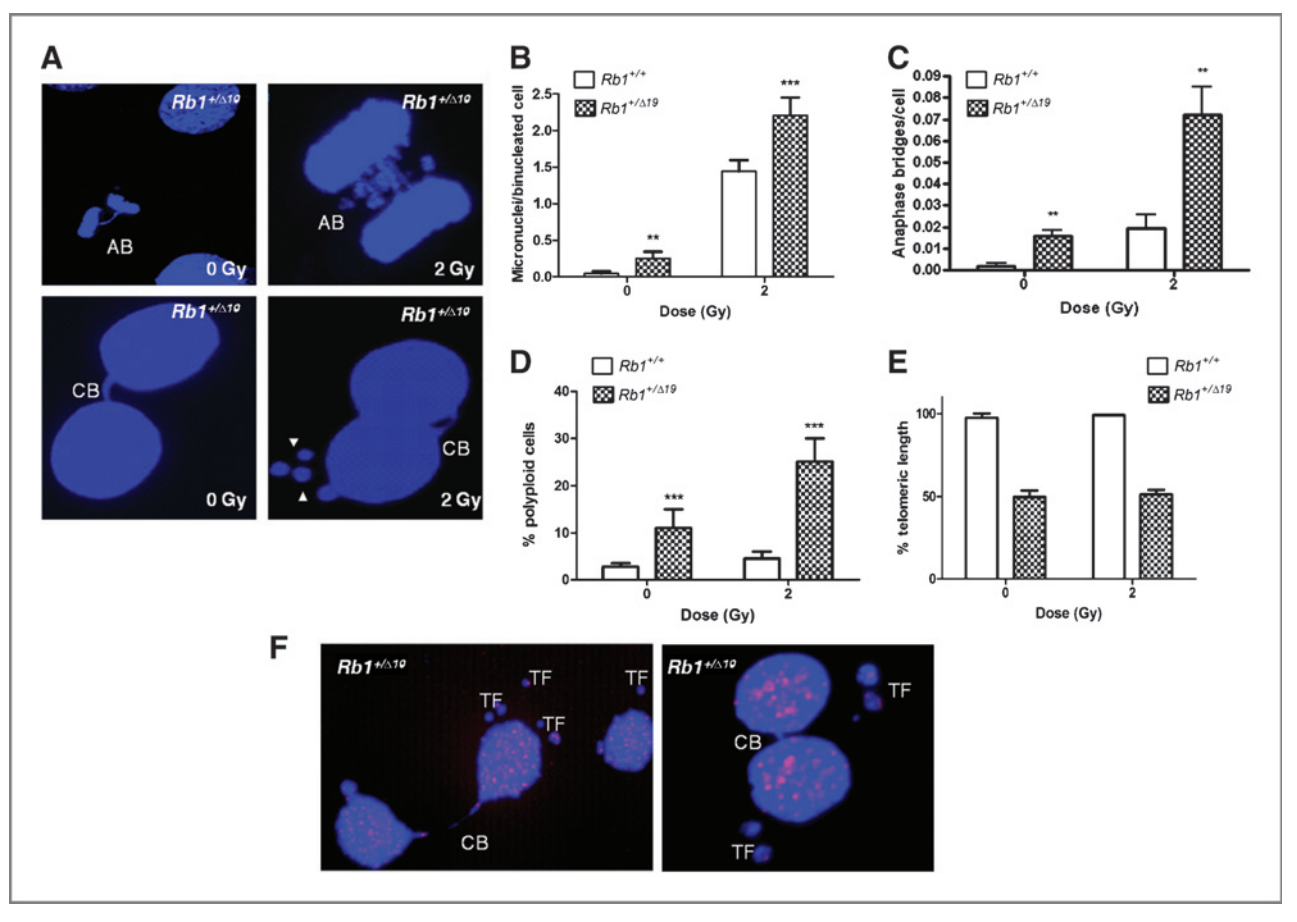


Figure 5. Radiation-induced genomic instability in $Rb1^{+/\Delta19}$ osteoblasts. A, left panels, compromised divisions: (left) anaphase bridges (AB) and chromatin bridges (CB; left) detected in DAPI-labeled nuclei of unirradiated $Rb1^{+/\Delta19}$ osteoblasts; right panels, anaphase bridges (AB) and chromatin bridges (CB) detected in DAPI-labeled nuclei of irradiated $Rb1^{+/\Delta19}$ osteoblasts. Arrowheads depict acentric fragments (micronuclei). B, radiation induced acentric DNA (micronucleus) fragments induced 24 hours after a 2 Gy acute exposure. Data are from 3 biological replicates. C, quantification of anaphase bridges and chromatin bridges induced 24 hours after a 2 Gy acute exposure. Data are from 3 biological replicates. D, polyploidy induced by radiation exposure. Increase in the polyploid population in $Rb1^{+/\Delta19}$ cells 24 hours after exposure to 2 Gy; data arising from cell-cycle flow analysis at passage 8. Data are from 2 biological replicates. Cells with a DNA content that was higher than 2N were considered to be aneuploid. E, telomeric length measured by Flow-FISH 48 hours after an acute 2 Gy radiation exposure. Data from 3 biological replicates of cells grown at passage 8 were used for this experiment. F, PNA stained chromatin bridges. Two representative images revealing chromatin bridges (CB) and telomere-containing acentric fragments 48 hours after exposure to 2 Gy in $Rb1^{+/\Delta19}$ osteoblasts at passage 12. ** and ***, P < 0.001 using Student's t test (ANOVA for anaphase bridges).

to prevent the continued increase in instability. These observations are consistent with a role for Rb1 in maintaining telomere integrity and ultimately genomic stability.

Reduced telomere length is closely associated with increasing numbers of completed cell cycles. This raises the formal possibility that the shortened telomeres in haploinsufficient $Rb1^{+/\Delta 19}$ cells may have arisen through accelerated cell division. However, no proliferation-promoting mutations were detected in the tumor suppressor genes Cdkn2a/Arf and p53 nor alterations of copy number changes in the oncogene Mdm2 or in the remaining wild-type Rb1 allele. Thus, there is only a small likelihood of expansion of a rapidly proliferating clone of mutant cells. Moreover, the *in vitro* deletion of the floxed Rb1 allele by lentiviral-mediated expression of the Cre-recombinase resulted in telomere loss within 3 passages. Wild-type cells would require more than 12 passages to reduce telomere length to that induced 3 passages after the loss of the floxed Rb1

allele, making it unlikely that telomeric losses can be explained simply by increased proliferation.

A direct action of the Cre recombinase on telomere length can also be excluded as the collagen transgene–driving Cre expression is not active in the undifferentiated osteoblast cells studied *in vitro*, leading to undetectable levels of *Cre* in these cells (16). The presence of lentiviral expressed Cre recombinase also had no effect on the telomere length of wild-type cells, indicating that the recombinase plays no part in the telomere shortening. The telomere reduction showed a consistent relationship to the copy number of the *Rb1* gene, with attrition increasing further when the remaining wild-type allele was targeted by shRNA knockdown, and reduced attrition when the deficiency in retinoblastoma was reversed by expression of *RB1*.

Exposure of haploin sufficient $RbI^{+/\Delta I9}$ cells to ionizing radiation raised the level of instability, as indicated by increases in the polyploid fraction, in failed chromosomal segregation, and the appearance of acentric DNA fragments. All 3 parameters reveal levels of instability that are far above those that are induced by the exposure of wild-type cells to radiation. The presence of telomeric DNA within both acrocentric fragments and anaphase bridges in irradiated cells suggests involvement of the shortened telomeres. This is consistent with the formation and breakage of end-to-end fusions between chromosomes capped by truncated telomeres or between truncated telomeres and radiation-induced double-strand breaks (23, 24). Such fused chromosomes would be subject to physical tension at the next cytokinesis, causing random breakage with the potential to form chromatin bridges and micronuclear fragments during the next cell cycle (25). Such repeated cycles of breakage-fusion-breakage (BFB) would continually increase the level of instability, as we have observed in the haploinsufficient $Rb1^{+/\Delta 19}$ cells. In support of this, we observed that telomere length was unaffected by radiation exposure. This indicates that the increased instability arises due to the combination of the induced DNA damage and the preexisting truncated telomeres.

The loss of one copy of the Rb1 gene, and the resultant haploinsufficiency, impaired the ability of the cells to handle radiation-induced stress by either G₂-M arrest or senescence. Impairment of both of these Rb1-dependent DNA damagerestoring functions that follow cell stress (23, 26, 27) may explain the persistence polyploid cells generated by the increased genomic instability. The concomitant loss of the canonical cell-cycle regulatory function of Rb1 would prevent cells with chromosomal damage from entering G1-S arrest and subsequently entering the apoptosis or senescence pathways. This sequence of events is consistent with the existence of a mutator phenotype originally proposed by Loeb (28) to explain the appearance of mutations in tumor cells at a rate above that predicted from the sporadic mutation rate alone. The duality of action (cell cycle and telomere length) that we ascribe to Rb1 can explain the increases susceptibility to both sporadic and radiation-induced osteosarcoma that is associated with retinoblastoma gene mutations (4, 6). This may also give an explanation for the high levels of chromosomal rearrangements that is frequently observed in osteosarcoma, and more recently in retinoma before the loss of the second *RB1* allele (12).

Another major component of the Rb1 pathway, P16INK4A, has been shown to promote telomere erosion, formation of anaphase bridges, and genomic instability in tumors of epithelial origin (29). The function of the retinoblastoma gene product in maintaining genomic instability has been suggested to involve chromosome condensation (30), centromere function, and mitosis-related genomic instability (31, 32). However, these previous studies indicate an apparently paradoxical situation, where loss of the retinoblastoma family members p107 and Rb2/p130, but not of Rb1 itself, were seen to promote telomere lengthening (33, 34). This prompts us to speculate that there is a balance between mutually antagonistic interactions of the retinoblastoma family of proteins that serve to regulate telomeric length.

Disclosure of Potential Conflicts of Interest

No potential conflicts of interest were disclosed.

Authors' Contributions

 $\textbf{Conception and design:} \ M.J. \ Atkinson, I. \ Gonzalez-Vasconcellos, M. \ Rosemann \\ \textbf{Development of methodology:} \ I. \ Gonzalez-Vasconcellos$

Acquisition of data (provided animals, acquired and managed patients, provided facilities, etc.): I. Gonzalez-Vasconcellos, M. Rosemann

Analysis and interpretation of data (e.g., statistical analysis, biostatistics, computational analysis): M.J. Atkinson, N. Anastasov, I. Gonzalez-Vasconcellos, M. Rosemann

Writing, review, and/or revision of the manuscript: M.J. Atkinson, I. Gonzalez-Vasconcellos

Administrative, technical, or material support (i.e., reporting or organizing data, constructing databases): O. Klymenko, B. Sanli-Bonazzi Study supervision: M.J. Atkinson, M. Rosemann

Grant Support

The studies are partly funded by grant 02NUK002E of the Bundesministerium für Bildung und Forschung. The funders had no role in study design, data collection and analysis, decision to publish, or preparation of the manuscript.

The costs of publication of this article were defrayed in part by the payment of page charges. This article must therefore be hereby marked advertisement in accordance with 18 U.S.C. Section 1734 solely to indicate this fact

Received August 28, 2012; revised March 20, 2013; accepted April 8, 2013; published Online First May 16, 2013.

References

- Mullenders L, Atkinson M, Paretzke H, Sabatier L, Bouffler S. Assessing cancer risks of low-dose radiation. Nat Rev Cancer 2009;9: 506, 604
- Fry SA. Studies of U.S. radium dial workers: an epidemiological classic. Radiation Res 1998:150:S21–9.
- Schmitt E, Ruckbeil C, Wick RR. Long-term clinical investigation of patients with ankylosing spondylitis treated with 224Ra. Health Phys 1983:44 Suppl 1:197–202.
- Eng C, Li FP, Abramson DH, Ellsworth RM, Wong FL, Goldman MB, et al. Mortality from second tumors among long-term survivors of retinoblastoma. J Natl Cancer Inst 1993:85:1121–8.
- Evans RD. The radium standard for boneseekers—evaluation of the data on radium patients and dial painters. Health Phys 1967;13: 267,79
- Gonzalez-Vasconcellos I, Domke T, Kuosaite V, Esposito I, Sanli-Bonazzi B, Nathrath M, et al. Differential effects of genes of the Rb1 signalling pathway on osteosarcoma incidence and latency in

- alpha-particle irradiated mice. Radiat Environ Biophys 2011;50: 135–41.
- Hanahan D, Weinberg RA. Hallmarks of cancer: the next generation. Cell 2011;144:646–74.
- Rosemann M, Kuosaite V, Kremer M, Favor J, Quintanilla-Martinez L, Atkinson MJ. Multilocus inheritance determines predisposition to alpha-radiation induced bone tumourigenesis in mice. Int J Cancer 2006:118:2132–8.
- Hu N, Gutsmann A, Herbert DC, Bradley A, Lee WH, Lee EY. Heterozygous Rb-1 delta 20/+ mice are predisposed to tumors of the pituitary gland with a nearly complete penetrance. Oncogene 1994;9:1021-7.
- Henson JD, Hannay JA, McCarthy SW, Royds JA, Yeager TR, Robinson RA, et al. A robust assay for alternative lengthening of telomeres in tumors shows the significance of alternative lengthening of telomeres in sarcomas and astrocytomas. Clin Cancer Res 2005:11:217–25.

- Artandi SE, DePinho RA. Telomeres and telomerase in cancer. Carcinogenesis 2010;31:9–18.
- Dimaras H, Khetan V, Halliday W, Orlic M, Prigoda NL, Piovesan B, et al. Loss of RB1 induces non-proliferative retinoma: increasing genomic instability correlates with progression to retinoblastoma. Hum Mol Genet 2008;17:1363–72.
- Marino S, Vooijs M, van Der Gulden H, Jonkers J, Berns A. Induction of medulloblastomas in p53-null mutant mice by somatic inactivation of Rb in the external granular layer cells of the cerebellum. Genes Dev 2000:14:994–1004.
- Dacquin R, Starbuck M, Schinke T, Karsenty G. Mouse alpha1(I)collagen promoter is the best known promoter to drive efficient Cre recombinase expression in osteoblast. Dev Dyn 2002;224:245–51.
- Soriano P. Generalized lacZ expression with the ROSA26 Cre reporter strain. Nat Genet 1999:21:70–1.
- Siggelkow H, Rebenstorff K, Kurre W, Niedhart C, Engel I, Schulz H, et al. Development of the osteoblast phenotype in primary human osteoblasts in culture: comparison with rat calvarial cells in osteoblast differentiation. J Cell Biochem 1999:75:22–35
- 17. Fenech M, Chang WP, Kirsch-Volders M, Holland N, Bonassi S, Zeiger E, et al. HUMN project: detailed description of the scoring criteria for the cytokinesis-block micronucleus assay using isolated human lymphocyte cultures. Mutat Res 2003:534:65–75.
- Azzalin CM, Reichenbach P, Khoriauli L, Giulotto E, Lingner J. Telomeric repeat containing RNA and RNA surveillance factors at mammalian chromosome ends. Science 2007;318:798–801.
- Cabuy E, Newton C, Roberts T, Newbold R, Slijepcevic P. Identification of subpopulations of cells with differing telomere lengths in mouse and human cell lines by flow FISH. Cytometry 2004;62:150–61.
- Lois C, Hong EJ, Pease S, Brown EJ, Baltimore D. Germline transmission and tissue-specific expression of transgenes delivered by lentiviral vectors. Science 2002;295:868–72.
- 21. Anastasov N, Bonzheim I, Rudelius M, Klier M, Dau T, Angermeier D, et al. C/EBPbeta expression in ALK-positive anaplastic large cell lymphomas is required for cell proliferation and is induced by the STAT3 signaling pathway. Haematologica 2010;95:760–7.

- 22. Vooijs M, Berns A. Developmental defects and tumor predisposition in Rb mutant mice. Oncogene 1999;18:5293–303.
- Tusell L, Pampalona J, Soler D, Frias C, Genesca A. Different outcomes of telomere-dependent anaphase bridges. Biochem Soc Trans 2010; 38:1698–703
- 24. McClintock B. The stability of broken ends of chromosomes in Zea Mays. Genetics 1941;26:234–82.
- Genesca A, Pampalona J, Frias C, Dominguez D, Tusell L. Role of telomere dysfunction in genetic intratumor diversity. Adv Cancer Res 2011;112:11–41.
- Chicas A, Wang X, Zhang C, McCurrach M, Zhao Z, Mert O, et al. Dissecting the unique role of the retinoblastoma tumor suppressor during cellular senescence. Cancer Cell 2010;17:376–87.
- Naderi S, Hunton IC, Wang JY. Radiation dose-dependent maintenance of G(2) arrest requires retinoblastoma protein. Cell Cycle 2002;1:193–200.
- 28. Loeb LA. A mutator phenotype in cancer. Cancer Res 2001;61:3230-9.
- Pampalona J, Soler D, Genesca A, Tusell L. Telomere dysfunction and chromosome structure modulate the contribution of individual chromosomes in abnormal nuclear morphologies. Mutat Res 2010;683: 16–22
- Coschi CH, Martens AL, Ritchie K, Francis SM, Chakrabarti S, Berube NG, et al. Mitotic chromosome condensation mediated by the retinoblastoma protein is tumor-suppressive. Genes Dev 2010; 24:1351–63
- van Harn T, Foijer F, van Vugt M, Banerjee R, Yang F, Oostra A, et al. Loss of Rb proteins causes genomic instability in the absence of mitogenic signaling. Genes Dev 2010;24:1377–88.
- Manning AL, Longworth MS, Dyson NJ. Loss of pRB causes centromere dysfunction and chromosomal instability. Genes Dev 2010;24: 1364–76.
- **33.** Garcia-Cao M, Gonzalo S, Dean D, Blasco MA. A role for the Rb family of proteins in controlling telomere length. Nat Genet 2002;32:415–9.
- 34. Kong LJ, Meloni AR, Nevins JR. The Rb-related p130 protein controls telomere lengthening through an interaction with a Rad50-interacting protein, RINT-1. Mol Cell 2006;22:63–71.